J Mater Sci (2019) 54:2102–2121

Composites

Influence of hygrothermal aging on the durability and interfacial performance of pultruded glass fiber-reinforced polymer composites

Shulan Yang[1], Weiqing Liu[2,*], Yuan Fang[1,*], and Ruili Huo[1]

[1] College of Civil Engineering, Nanjing Tech University, Nanjing 211816, People's Republic of China
[2] Advanced Engineering Composites Research Center, Nanjing Tech University, Nanjing 211800, People's Republic of China

Received: 16 May 2018
Accepted: 20 September 2018
Published online: 1 October 2018

ABSTRACT

The influence of the fiber/matrix interface of pultruded glass fiber-reinforced polymer (GFRP) composites exposed to hygrothermal environments, including deionized water immersion and saltwater immersion at 20 ± 5 °C, 30 ± 1 °C, and 60 ± 1 °C for 180 days, was investigated. The effect of moisture absorption on tensile properties was discussed. After 180 days of immersion in deionized water, tensile strength and modulus of specimens decreased 25.7% and 26%, whereas the equivalent respective losses were 2.1% and 18.2% for specimens immersed in saltwater. The short-beam-shear test and the single-fiber fragmentation test were selected to reflect the degradation of macro- and micro-interfacial properties, respectively. After 180-day immersion in deionized water and saltwater at 60 ± 1 °C, the inter-laminar shear strength of specimens decreased 28.8% and 18.5%, respectively, and the corresponding interfacial shear strength decreased 53.2% and 23.5%, indicating that the diffusion rate of micro-interface was higher than that of macro-interface in the fiber direction. Immersion in all media leads to pronounced degradation in tensile strength, modulus, and inter-laminar shear strength. Furthermore, based on the change of interfacial strength and Weibull distribution, a prediction model was proposed to describe the degradation trends and temperature effects on ultimate bearing capacity of pultruded GFRP composites in hygrothermal environments.

Introduction

Fiber-reinforced polymer (FRP) composites, especially glass fiber-reinforced polymer (GFRP) composites [1–3], have been widely used in civil engineering applications as a competitive alternative to traditional materials due to their characteristics, namely lightness, high strength, ease of installation, and corrosion resistance. Pultrusion of FRP is a particularly easy method that can produce continuous lengths of constant cross-sectional shapes at relatively low cost. This material is suitable to be used to

Address correspondence to E-mail: wqliu@njtech.edu.cn; yuanfang@njtech.edu.cn

https://doi.org/10.1007/s10853-018-2944-6

fabricate a structural profile for civil engineering application, in both new construction and rehabilitation of degraded infrastructure [4]. One of the most important fields of application of FRP profiles is the replacement of reinforced concrete or steel-deteriorated bridge decks. However, during their service life, these materials, especially in an outdoor environment, are inevitably exposed to high temperatures and high moisture (either in the form of rain or atmospheric vapor). The water uptake in FRP composites exposed to hot/wet conditions would lead to the reduction of the glass transition temperature (T_g) of FRP composites and the degradation of mechanical properties of FRP composites [5]. Therefore, it is important to understand how the behavior and performance of pultruded GFRP composites are affected by the in-service hygrothermal environments.

Numerous studies have been carried out on the mechanical properties and long-term durability of FRP composites under hygrothermal environments [6–8]. Silva et al. [9] investigated the mechanical properties of E-glass fiber/epoxy resin laminates after immersion in a 5% NaCl solution kept at three different temperatures: 35 °C, 50 °C, and 65 °C. After immersion for 5,000 h, the ultimate strain increased 1.8% at 30 °C, while decreased 3.84% at 40 °C and 14.7% at 55 °C. In addition, the elasticity modulus decreased 14.1, 12.2, and 7.5% at 30 °C, 40 °C, and 55 °C, respectively. Similar observations were made by Guermazi et al. [10] in which the tensile strength and Young's modulus were affected by hygrothermal aging. The tensile strength and Young's modulus of glass fiber-reinforced epoxy composites decreased 27% and 20% of their initial values, respectively, after 90 days immersed in distilled water at 24 ± 3 °C, while the reductions of tensile strength and Young's modulus were 31% and 26%, respectively, after 90 days immersed in distilled water at 90 °C. Furthermore, Grammatikos et al. [4] investigated the effects of hygrothermal aging on the durability of pultruded glass fiber-reinforced isophthalic polyester composites immersed in distilled water at 25 °C, 40 °C, 60 °C, or 80 °C for a period of 224 days. They found that the tensile strength and shear strength of pultruded FRP composites reduced by ~ 16% and ~ 31% after 224 soaking days at 80 °C.

Although the researches on the mechanical properties and long-term durability of FRP composites have been conducted, to some extent the effect of hygrothermal environments on the interfacial performance between fiber and matrix is limited. Gu et al. [11] investigated the changes of macro- and micro-interfacial properties of carbon fiber/epoxy resin composites under hygrothermal treatments based on a short-beam-shear (SBS) test and a single-fiber fragmentation test (SFFT). They found that the inter-laminar shear strength (ILSS) and interfacial fracture energy (Γ_i) of CF-1/5228 composites decreased by 11% and 52%, respectively, when exposed to water at 70 °C for 7 days. Ramirez et al. [12] evaluated water degradation of FRP composites by SFFT tests based on energy-based model. They concluded that specimens subjected to seawater at 60 °C showed more loss of fiber/matrix interface shear strength (~ 75%) for 1300 h compared to those exposed to seawater at 40 °C (~ 69%). In the study of Sousa et al. [5], the pultruded GFRP profiles were exposed to thermal cycles (− 5 to 40 °C) for 190 cycles. They found that changes in T_g and mechanical properties were less significant when compared to those caused by hygrothermal aging. Scanning electron microscopy (SEM) results indicated that thermal cycles aging had two main consequences in GFRP pultruded specimens: some degradation of the fiber/matrix interface and some degradation of the matrix itself.

As described above, many studies have been carried out on the durability of FRP composites. However, to the best of our knowledge, there has been little report on the degradation mechanism of FRP composites in the hygrothermal environment based on both the spectroscopic and microstructural analyses. This study analyzed the degradation mechanism of pultruded GFRP composites in the hygrothermal environment from a microstructural view using scanning electron microscope (SEM) and Fourier transform infrared spectroscopy (FTIR) analyses of the changes in microstructures and chemical structures. Moreover, in this study, the effects of hydrothermal environments on the macro- and micro-mechanical properties were explored. Additionally, an analytical model depended on Weibull distribution of debonding strength between single fiber and matrix, considered the effect of hygrothermal aging, was developed to predict the long-term tensile performance of pultruded FRP composites.

Experimental details

Materials

Unidirectional E-glass fiber of 24 μm diameters and tensile strength of 2991 MPa, in the form of EDR480-T910, were manufactured by Mount Tai Glass Fiber Co., Ltd, China. Isophthalic unsaturated polyester resin was supplied by Jinling DSM Resins Co., Ltd, China. Based on tests of unreinforced resin plates, the tensile strength and modulus were determined to be 62 MPa and 3.4 GPa. Furthermore, T_g of isophthalic unsaturated polyester resin was 87 °C. Benzoyl peroxide (BPO) and tert-butyl perbenzoate (TBPB) were purchased from Aldrich, which represent the 0.6% and 1.2% of weight, respectively. As oxidant initiators, they can initiate the curing reaction of isophthalic unsaturated polyester resin. All chemicals were used as received, without further purification.

Composite processing

Pultruded rectangular laminates have been produced using unidirectional E-glass fiber and isophthalic unsaturated polyester resin. The fiber volume fraction is ≈ 60% for the components, of which ≈ 50% is unidirectional roving and ≈ 10% is fabric (0°/90°) around unidirectional roving. Both TBPB and BPO have been used as curing agents, which represent 0.6% and 1.2% of weight, respectively. Heat deflection temperature (HDT) for the resins measured by the producer is 110 °C. In the heated molds, the temperature 110 °C was set to make the surface of specimen obtain ≈ 95% of complete polymerization inside the mold. It was verified by testing the polymerization with the resin powder obtained from the surface of the specimen with differential scanning calorimetry (DSC). Laminate thickness was 2.7 mm.

Hygrothermal aging

Specimens were immersed to deionized water and saltwater for 15, 30, 60, 90, 120, and 180 days at 30 ± 1 °C and 60 ± 1 °C, respectively. The saltwater was formulated as described by Chin et al. [13]. The saltwater solution comprised of 3.5% by mass sodium chloride (3.5% NaCl) and deionized water. In addition, another two groups of the specimens aged in solution at 20 ± 5 °C for 180 days. An unexposed condition (storage in a room environment) was set to represent control condition.

Absorption tests

Water absorption measurements were taken by gravimetric analysis according to ASTM D5229 [14]. The specimens were harvested from the immersion tank, wiped to remove surface moisture, kept in room environment for 2 h, and then weighed to monitor the mass change periodically. At least five specimens sized as 250 mm long, 25 mm wide, and 2.7 mm thick were tested for each condition. (See details in Table 1.) The moisture absorption M_t of the samples was calculated using the following equation:

$$M_t = 100\left(\frac{W_t - W_0}{W_0}\right) \quad (1)$$

where W_t is the specimen weight at time t and W_0 is the dry weight of the untreated dry specimen.

Tensile tests

The ultimate tensile properties of the composites were determined by standardized static tension tests in accordance with ASTM D3039 (type C) [15]. (See details in Table 1.) Each specimen was 250 mm long, 25 mm wide, and 2.7 mm thick with 1.5-mm-thickness aluminum tabs, as shown in Fig. 1, bonded at both ends of the GFRP profiles to minimize stress concentrations near the gripping zone before tensile tests. Then, the holding area of the specimens was clamped to be loaded by friction force, and uniform tension field is formed in the working section. The tensile tests were carried out after 15, 30, 60, 90, and 180 days of immersion. At least five specimens for each condition were tested using a universal testing machine (model CSS-44100) produced by Changchun Research Institute, with the load cell of 50-kN capacity and the test speed of 2 mm/min. An extensometer was used to monitor the strain of the specimens. All specimens were tested in the fiber direction, which is basically less susceptible to fiber/matrix interface and matrix damage. All specimens were tested at 20 ± 5 °C and 75% relative humidity (RH).

Table 1 Outline of the experimental details of the tests

Test types	Specimen types	Dimensions of specimens (mm)	Number of specimens per group	Temperature (°C)	Immersion environment	Immersion time (days)
Absorption test	Pultruded GFRP laminates	250 × 25 × 2.7	5	20 ± 5, 30 ± 1, 60 ± 1	Deionized water, saltwater	180
Tensile test	Pultruded GFRP laminates	250 × 25 × 2.7	5	20 ± 5	Deionized water, saltwater	180
SBS test	Pultruded GFRP laminates	16.2 × 5.4 × 2.7	20	30 ± 1, 60 ± 1	Deionized water, saltwater	180
SFFT	dumbbell-shaped SFFT sample	–	20	30 ± 1, 60 ± 1	Deionized water, saltwater	180
SEM test	Pultruded GFRP laminates	250 × 25 × 2.7[a]	1	20 ± 5	Deionized water, saltwater	180
FTIR test	Pultruded GFRP laminates	250 × 25 × 2.7[b]	1	30 ± 1, 60 ± 1	Deionized water, saltwater	180

[a]Before SEM tests for pultruded GFRP laminates, specimens were cut into thin films along the section perpendicular to the fiber and the section parallel to the fibers, respectively

[b]Before FTIR test for pultruded GFRP laminates, specimens were ground into powders

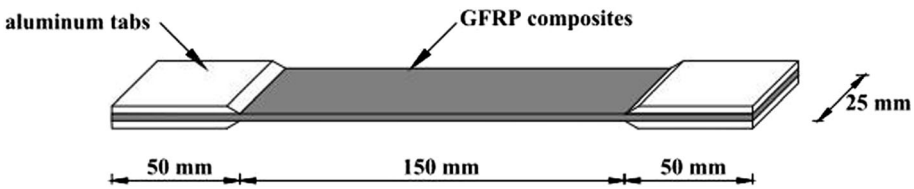

Figure 1 Test coupon of GFRP tensile test.

Short-beam-shear (SBS) test

The short-beam-shear test is a widely used method for characterizing the inter-laminar failure resistance of FRP composites. This test method involves loading a beam under three-point bending with the special dimensions such that an inter-laminar shear failure is induced. The apparent inter-laminar shear strength can be measured from this method [16]. Five test coupons for each material were cut along the unidirectional laminate composites for an inter-laminar shear strength test, according to standard ASTM D2344 [17]. The Zwick/Roell universal testing machine was used with a loading rate of 1 mm/min (Fig. 2). The diameters of the loading nose and side supports were 6 mm and 3 mm, respectively. And the strain was tested by setting the strain gauge on the upper surface of specimens at the support position. The size of the specimens for short-beam-shear test was 16.2 mm × 5.4 mm × 2.7 mm, at a span length of 12 mm. All specimens were tested at

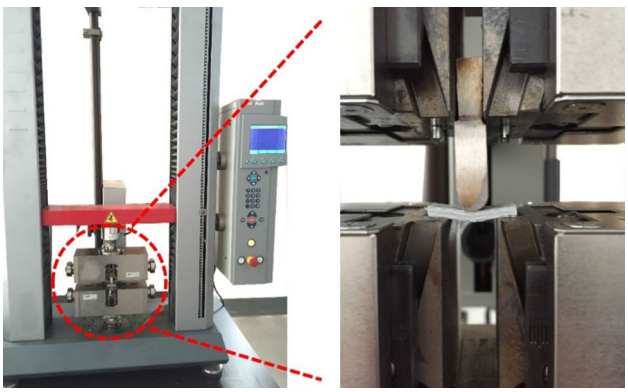

Figure 2 Experimental setup for short-beam-shear test.

20 ± 5 °C and 75% relative humidity (RH). The ILSS value can be calculated by Eq. (2).

$$\mathrm{ILSS} = \frac{3P_b}{4bh} \tag{2}$$

where P_b is the maximum failure load, and b and h are the sample's width and thickness, respectively.

Single-fiber-fragment test (SFFT)

The fragmentation test was developed from the early work of Kelly and Tyson, who investigated brittle tungsten fibers that broke into multiple segments in a copper matrix composite [18]. Depending on the level of fiber/matrix adhesion, such tensile forces are transferred from the matrix to fiber. The higher the axial strain, the more fractures will be caused in the fiber (Fig. 3a). The calculation of the interfacial shear strength τ was carried out according to the following equation:

$$\tau = \frac{\sigma_f}{2}\left(\frac{d}{l_c}\right) \quad (3)$$

where σ_f is the fiber strength at the critical length, d is the fiber diameter, and l_c is the critical fragment length of fiber.

The critical fiber length is defined as the shortest fragment length that breaks due to a stress application. We determined this using the following equation:

$$l_c = \frac{4}{3} \times \overline{L} \quad (4)$$

where $\overline{L}$ is the average fragment length.

A single fiber was put in the middle of a high-temperature-resistant silicone mold with a metal weight of 10 g at each end of the fiber to pre-strain it. Weights of 10 g imparted a pre-strain of about 0.65% for a typical glass fiber. The fiber was then filled with isophthalic unsaturated polyester resin using a pipette. After curing at 20 ± 5 °C for 6 h, it was moved into an oven at 80 °C for 1 h. The dumbbell-shaped SFFT sample can be seen in Fig. 3(b). The SFFT test was tensioned with a cross-speed of 1 mm/min using the Zwick/Roell universal testing machine, with a load cell of 20-kN capacity (Fig. 4). And at least 20 specimens for each condition were tested. (See details in Table 1.) When the specimen is broken into two parts, they will be observed under an optical microscope. The break points of the fiber will be marked one by one. Then, the distance between two adjacent points is the length of fiber fragments. The fiber inside the resin broke into increasingly smaller fragments at locations where the fiber's axial stress reached its tensile strength.

Scanning electron microscopy (SEM)

SEM observations and image analysis were performed with a QUANTA 200 (Philips-FEI, Holland) to observe the microstructure of specimens before and after aging. Samples were taken from unconditioned specimens and specimens that were aged in deionized water and saltwater at 20 ± 5 °C for 30, 90, and 180 days, respectively. (See details in Table 1.)

Fourier transform infrared spectroscopy (FTIR)

To further identify the changes of chemical structures of pultruded FRP composites before and after hydrothermal aging. (See details in Table 1.) FTIR spectra were recorded on a Nicolet-6700 spectrometer from Thermo Electron. The powders were ground into a dry KBr pellet. In all cases, 32 scans in the 400–4000 cm^{-1} region at a resolution of 4 cm^{-1} were used to record the spectra.

Introduction of the theory analysis

In Coleman's [19] study, the integrated intensity distribution function of fiber $P_f(\sigma_f)$ can be well described by the use of the Weibull distribution. At the same time, the strength of single fiber and the strength of fiber bundle can be interchanged if the following assumptions are satisfied.

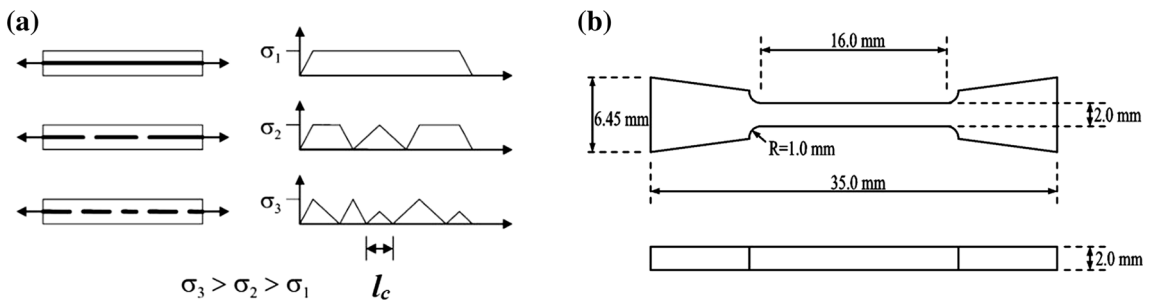

Figure 3 **a** Schematic representation and **b** test coupon of the single-fiber-fragment test coupon.

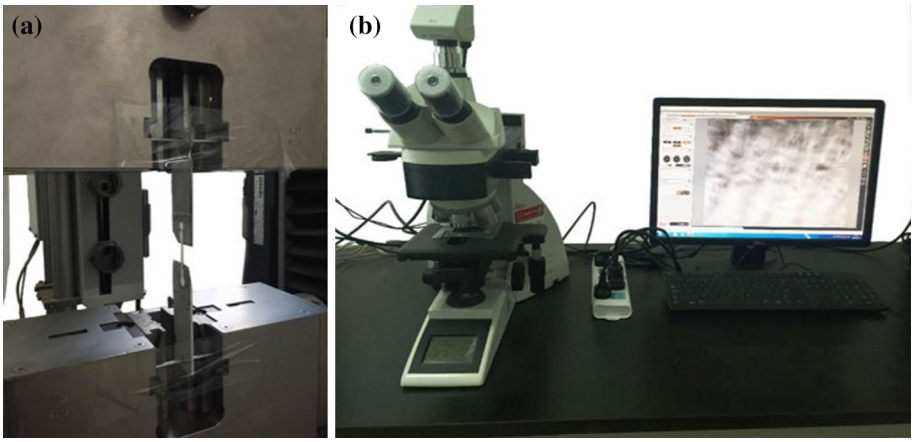

Figure 4 Experimental setup for single-fiber-fragment test: **a** experimental setup and **b** optical microscope.

1. The tensile strength of fiber is subject to Weibull distribution function, which is described in form as

$$P_f(\sigma_f) = 1 - \exp\left[-L\left(\frac{\sigma_f}{\sigma_0}\right)^{\alpha}\right] \tag{5}$$

where $P_f(\sigma_f)$ is the failure probability when the stress level is equal to or less than σ_f. L is a length ratio about a reference length. σ_0 is the scale parameter when $L = 1$. α is the shape factor. It is must be mentioned that all of the parameters are material constants and usually determined by test.

2. Also, the stress σ_f and strain ε_f of single fiber obey the Hooke's law, formed as

$$\sigma_f = E_f \varepsilon_f \tag{6}$$

where E_f is the elasticity modulus of fiber.

3. During the tensile test of fiber bundle, the applied load was uniformly distributed to the effective fiber at any time.
So that, the relationship between tensile load and strain (F–ε) can be established as

$$P_f(\varepsilon_f) = 1 - \exp\left[-L\left(\frac{\varepsilon_f}{\varepsilon_0}\right)^{\alpha}\right] \tag{7}$$

where ε_0 is the scale parameter when $L = 1$, and $\varepsilon_0 = \sigma_0/E_k$

It is assumed that the strain of fiber changed evenly in pultruded GFRP composites, and a number of effective fibers are defined as N_0, when the total number of fibers in composite profile is N. And N_0 is given as

$$N_0 = N[1 - P_f(\varepsilon_f)] = N\exp\left[-L\left(\frac{\varepsilon_f}{\varepsilon_0}\right)^{\alpha}\right] \tag{8}$$

In most cases the number of effective fibers is related to the tensile load F, and the relationship is given as

$$F = \sigma_f A_f N_0 \tag{9}$$

where A_f is the cross-sectional area. Substituting Eqs. (5) and (8), respectively, into Eq. (9) gives

$$F = A_f E_f \varepsilon_f N \exp\left[-L\left(\frac{\varepsilon_f}{\varepsilon_0}\right)^{\alpha}\right] \tag{10}$$

Results and discussion

Moisture absorption

Figures 5 and 6 show the effects of immersion time in deionized water and saltwater on the moisture absorption of pultruded GFRP composites during 180 days of aging under different temperatures. The moisture absorption curves indicated a multistage process. The data increased linearly with time at initial diffusion stage, which appeared to follow Fick's law. However, when immersion time increased, a dramatic mass loss can be found in specimens immersed in both deionized water at 20 ± 5 °C and seawater at all three temperatures, which deviated from Fick's law. The loss of the material was due to a dehydration reaction following hydrolysis when the specimens were in both water and saltwater conditions, which will be discussed in "FTIR analysis " section.

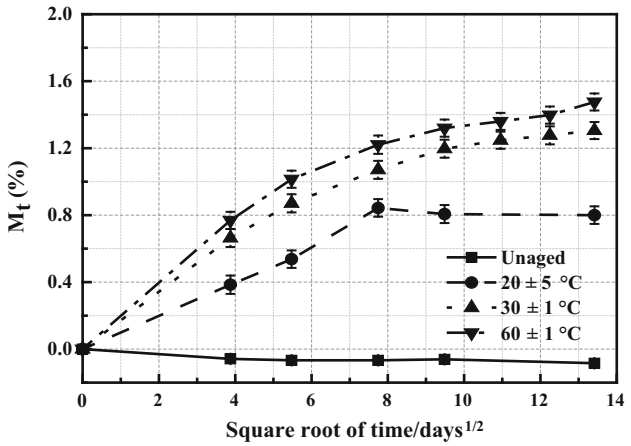

Figure 5 Moisture absorption curves of pultruded GFRP composites immersed in deionized water.

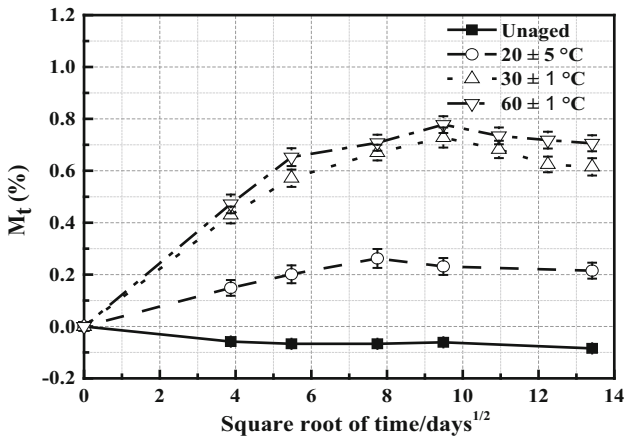

Figure 6 Moisture absorption curves of pultruded GFRP composites immersed in saltwater.

At an immersion time of 60 days, the moisture absorption of specimens in deionized water and saltwater at 20 ± 5 °C was 0.84% and 0.26%, respectively. Instead, the mass loss in saltwater at 30 ± 1 °C and 60 ± 1 °C happened after 90 days, and the moisture absorption of specimens at 30 ± 1 °C and 60 ± 1 °C was 0.72% and 0.78%. The result suggested that the equilibrium moisture absorption in seawater was slightly lower than that in deionized water, which was consistent with the results reported in the previous literature [20–22]. Also, the increase of immersion temperature accelerated the level of moisture absorption and greatly shortened the moisture saturation time, which was consistent with results reported by Xian [23] and Firdosh [24]. However, when pultruded GFRP composites immersed in deionized water at 30 ± 1 °C and 60 ± 1 °C, no saturation plateau was found after extended immersion time. At an immersion time of 180 days, the maximum moisture absorption was 1.3% and 1.48%, respectively. Similar behavior has been observed in a previous study by Xin et al. [25] who reported that the water absorption of GFRP composites immersed in water at 65 °C kept rising after 6 months and began to decrease after 14 months.

Table 2 lists the overall results in terms of maximum moisture absorption over the 180-day period of investigation, diffusion coefficient, and the activation energy for diffusion determined from the moisture absorption curves. During the detection period, when the average moisture absorption of the material is less than 0.01%, the material is considered to have reached the effective equilibrium moisture absorption. Uncertainty in table is showed by the standard deviation, "S", from laboratory average data. The initial part of the moisture absorption curves can satisfy $\sqrt{Dt}/h \leq 0.28$, and the plate can be viewed as infinite in the plane directions with a large width-to-thickness ratio. The independent diffusion coefficient (D) was calculated as follows, according to a study by Shen and Springer [26]:

$$D = \pi\left(\frac{h}{4M_\infty}\right)^2\left(\frac{M_2 - M_1}{\sqrt{t_1} - \sqrt{t_2}}\right)^2 \tag{11}$$

where M_∞ is the equilibrium amount of absorption, h is the plate thickness, M_1 and M_2 are the amount of absorption at times t_1 and t_2, respectively, and $\frac{M_2 - M_1}{\sqrt{t_1} - \sqrt{t_2}}$ is the slope of the moisture absorption plot in the initial linear portion of the curve. The slope remains stable and is not affected by aging. A comparison with the values of moisture absorption and diffusion coefficient in Table 2 showed that the specimens immersed in deionized water had a larger diffusion coefficient (D) and higher value of moisture absorption than those obtained for specimens immersed in saltwater under the same condition. Chin et al. [14] reported a similar result which suggested that the presence of NaCl molecules in the diffusion of water played a role in decreasing the maximum moisture absorption at saturation. The reason was caused by the reverse osmosis phenomenon in which water entering into the composite formed electrolysis environment as it dissolved water-soluble substances within the polymer [27]. The activation energy for diffusion (E_d) provides an indication of the energy

Table 2 Characteristics of moisture absorption

Temperature (°C)	Immersion in deionized water				Immersion in saltwater			
	$M_{t\ =\ 180\ days}$ (%)	S(%)	D ($\times\ 10^{-7}$mm^2/s)	E (kJ/mol)	$M_{t\ =180\ days}$ (%)	S(%)	D ($\times\ 10^{-7}$mm^2/s)	E (kJ/mol)
20 ± 5	0.84	0.05	1.75	5.07	0.26	0.04	0.73	4.68
30 ± 1	1.30	0.05	2.00		0.72	0.04	1.40	
60 ± 1	1.48	0.05	2.40		0.78	0.03	1.66	

barrier that must be overcome for diffusion of moisture to take place, and can be determined using an Arrhenius type of relationship [28]:

$$D = D_0 \exp\left(\frac{-E_d}{RT}\right) \tag{12}$$

where D_0 is a constant coefficient, R is the universal gas constant (8.31 J/mol K), D is the diffusion coefficient, and T is the temperature (K). Plotting ln(D) versus ($1/T$), values of activation energy for the composites immersed in deionized water and saltwater are determined to be 5.07 and 4.68 kJ/mol K, respectively. The values are lower than those reported by Valadez-Gonzalesm [29] (≈ 8.6 kJ/mol with vinyl resin), Chu [30] (≈ 12.14 kJ/mol with vinyl resin), and Abanilla [31] (≈ 48.09 kJ/mol with epoxy resin). It can be noted that the activation energy is not only affected by the immersion conditions, but also influenced by the types of matrix. Moreover, the difference in the maximum moisture absorption at saturation indicated that pultruded GFRP composites immersed in deionized water would suffer more degradation because of the water aging, which would influence on the mechanical properties and the damage mechanisms [32]: hydrolysis of the matrix, chain breakage, creation of small molecules, and extraction out of these molecules from the composites.

Tensile behavior

The changes in the tensile strength and modulus of aged specimens versus time of immersion are shown in Figs. 7 and 8, and Table 3. A two-phase evolution of the tensile strength was observed. First, a consolidation phase showed an increase in the tensile strength under all exposed conditions. During this stage, the tensile strength of composites improved slightly due to the action of post-curing reaction [31]. As shown in Fig. 7, the tensile strength attained the top retention at 30 days. The strength increased 12.2, 21.2, and 14.0% for the control specimen and specimens immersed in deionized water and saltwater, respectively.

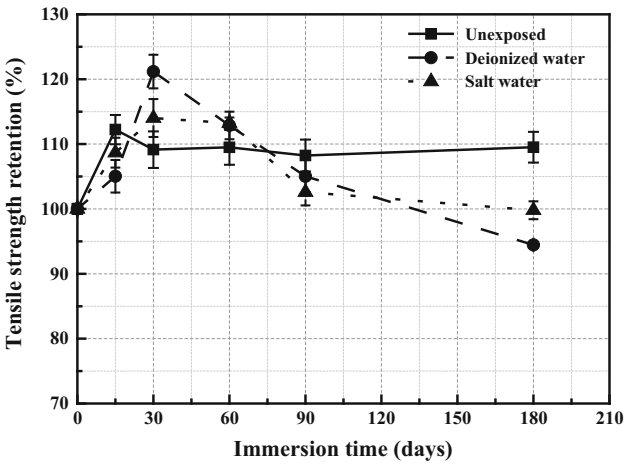

Figure 7 Tensile strength retention of pultruded GFRP composites versus immersion time for deionized water immersion and saltwater immersion at 20 ± 5 °C.

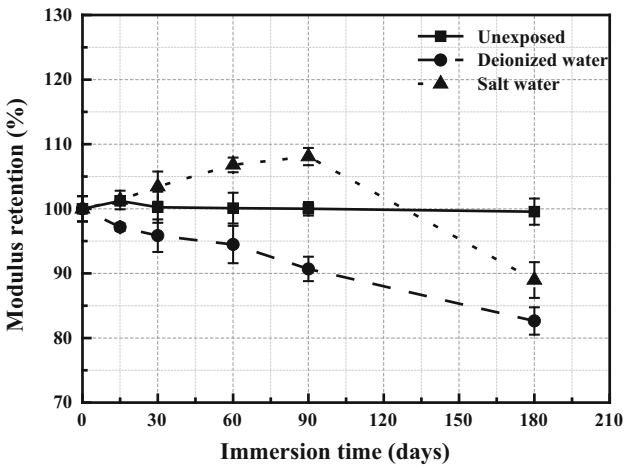

Figure 8 Tensile modulus retention of pultruded GFRP composites *vs.* immersion time for deionized water immersion and saltwater immersion at 20 ± 5 °C.

Table 3 Tensile properties of pultruded GFRP composite immersed in deionized water and saltwater

Time period (days)	Unexposed				Deionized water				Saltwater			
	Tensile strength (MPa)	S (MPa)	Elastic modulus (GPa)	S (GPa)	Tensile strength (MPa)	S (MPa)	Elastic modulus (GPa)	S (GPa)	Tensile strength (MPa)	S(MPa)	Elastic modulus (GPa)	S (GPa)
Unexposed tensile strength = 503.508 (MPa); unexposed tensile elastic modulus = 22.758 (GPa)												
15	556.214	11.359	23.038	0.036	520.595	12.653	22.111	0.129	565.053	11.586	23.067	0.328
30	540.912	14.174	22.811	0.548	600.551	13.011	21.812	0.573	508.483	14.693	23.540	0.531
60	542.730	13.544	22.781	0.541	559.384	10.674	21.500	0.657	538.553	4.285	24.305	0.258
90	536.395	12.366	22.759	0.238	520.451	15.045	20.631	0.429	561.241	10.312	24.598	0.305
180	542.747	11.933	22.658	0.460	468.075	18.893	18.807	0.482	494.613	6.928	20.249	0.628

After 30-day immersion, a degradation phase followed, which clearly exhibited a drastic drop of the tensile strength. Compared to unexposed specimens, the values of specimens immersed in saltwater decreased sharply before 90 days, and those immersed in deionized water decreased continuously as immersion time increased. The opposite behavior was observed by Kafodya [33]. In his study, the tensile strength decreased at the first stage and then increased as the immersion time progressed. The difference could be attributed to the effect of sustained loading in his study. Also, in Wellington Chu's study [30], there was just a degradation phase. The difference could be the effect of the different matrix system. Marouani et al. [34] pointed out that the duration of this phase depended on the aging environment and the nature of the composite matrix. After 180 days of immersion, the tensile strength retention was 109.5, 94.4, and 99.8% for un-aged specimens, specimens immersed in deionized water, and those immersed in saltwater, respectively.

Similarly, Fig. 8 shows that after 180 days, the tensile modulus retention was 99.6, 82.6, and 88.9% for un-aged specimens, specimens immersed in deionized water, and those immersed in saltwater, respectively. However, the changes in tensile modulus have no marked consolidation phase except when immersed in saltwater. It can be noted that higher moisture absorption in water is an important factor in the degradation of tensile properties. Moreover, the presence of NaCl molecules prevents the diffusion of water molecules from the matrix to the fibers, which leads to less degradation in the tensile property of specimens exposed to seawater. When water molecules contact with polymer, weak bonds form and water molecules diffuse through the material, resulting in swelling and polymer chains breaking. The separation of polymer chains reduces the polar attraction between chains and allows for increased chain mobility, resulting in diminished mechanical properties.

Multi-scale interfacial properties

SBS test and SFFT were employed to investigate changes in macro- and micro-interfacial properties, respectively. The level of fiber/matrix bond interface and resin may account for the majority of deterioration, as noted by Abanilla [31]. The ILSS test provides a simple way to rank environmental conditions based on their effects on the inter-laminar strength of GFRP composites. Overall results and variation tendency of short-beam strength for the composites immersed in deionized water and saltwater at different temperatures are shown in Fig. 9 and Table 4. As can be seen in Fig. 9, the ILSS values dropped in a stepwise fashion like that reported by Chu et al. [30]. However, when specimens immersed in either deionized water or saltwater at 30 ± 1 °C, the values were slightly increased at the initial phase due to residual post-cure. And the maximum raise was 4.2% at the end of first 15 days immersed in deionized water, and it was 4.7% at the end of the first 30 days in saltwater. Then, there was a steady decline, followed by a rapid drop over the rest of the exposure period. The results were indicative of an almost pure inter-laminar failure whereby changes in strength depended only on interfacial mechanisms without substantial physical/mechanical degradation of the matrix [30], whereas, instead of slight increases, there were continuous

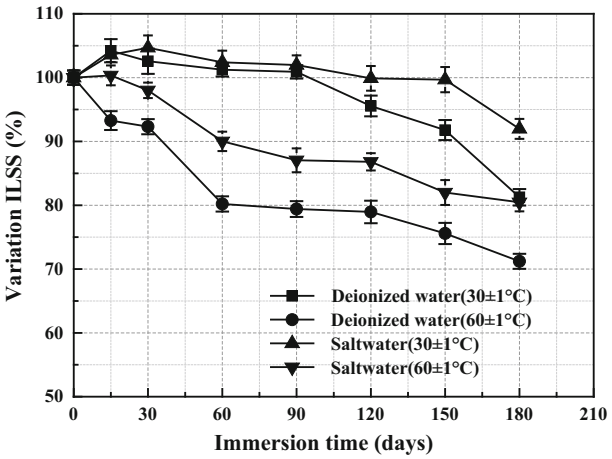

Figure 9 Inter-laminar shear strength retention of pultruded GFRP composites versus immersion time for deionized water immersion and saltwater immersion at different temperatures.

declines associated with all conditions at 60 °C. In all cases, the maximum drop (28.8%) occurred for specimens immersed in deionized water at 60 °C. At this temperature level, aging can be considered substantially accelerated under severe exposure conditions, as explained by Karbhari [28]. The minimum relative level of degradation was shown by composites immersed in saltwater at 30 ± 1 °C, with a drop of 8.9%. As mentioned above, this could be attributed to the effect of further polymerization, plasticization of the matrix, swelling, and release of internal stress [35]. Beyond this, degradation may also be caused by water, leading to hydrolysis reaction in both resin and fiber systems. The coalescence of micro-cracks to macro-cracks serves to enhance the wicking of moisture along the fiber.

Figure 10 shows typical failure images of pultruded GFRP composites in SBS test immersed in deionized water at 30 ± 1 °C and 60 ± 1 °C, respectively. As aging progressed, the main crack expanded and extended (Figs. 10a, c), and several small cracks were visible (Figs. 10b, d). Similar damage patterns were observed in the case of immersion in saltwater (Fig. 11). The failure of specimens in both conditions clearly started as a horizontal shear failure at mid-thickness in the form of a longitudinal crack, which propagated to the left or right with no preference along the neutral axis, as observed during testing. These results agreed with the findings in Sawpan's study [36]. However, when compared to the results in water condition, it was noted that there were thinner main cracks and fewer small cracks for specimens immersed in saltwater condition. These images again confirmed the test results, which showed that the specimens immersed in deionized water had a higher level of degradation than those immersed in saltwater.

The values from the SFFT in various immersion conditions are shown in Tables 5 and 6. Compared with the results for un-aged specimens, the specimens immersed in 30 ± 1 °C deionized water, 60 ± 1 °C deionized water, 30 ± 1 °C saltwater, and 60 ± 1 °C saltwater, respectively, needed higher tensile force and had more fiber fragments during the SFFT. The results indicated that the interfacial bond strength, which means the bond strength between fibers and matrix, decreased after aging. As seen in Fig. 12 and Table 5, the bond strength increased to 116.7% and 126.3% in the first 30 days and then declined to 78.9% and 99.5% after 180 days of immersion in deionized water and saltwater at 30 ± 1 °C, respectively. There were sharp decreases in the other two conditions, where the values of specimens immersed in deionized water and saltwater, both at 60 ± 1 °C, fell to 46.8% and 76.6%, respectively. Figure 13 shows the failure mode of the fibers and matrix of the specimens after the SFFT test. The break points of the fiber and the gaps due to slip can be clearly seen, while the distance between the two break points is the length of the broken fiber. The bonding strength values of specimens immersed in saltwater were significantly higher than those immersed in deionized water at the same temperature, and the reduction in the bonding strength of specimens immersed in 60 ± 1 °C water was more dramatic than those immersed in water at 30 ± 1 °C. The bonding strength of single-fiber composites changed in a similar manner to the ILSS results at the same condition. Thus, the ranks in interfacial resistance were the same based on the results from SBS and SFFT. Gu et al. [11] found a similar consistency of macro- and micro-interfacial bonding when evaluating the effects of immersion time and temperature on carbon fiber-reinforced epoxy resin composites.

Relationship between moisture absorption and the macro- and micro-interfacial properties

To compare the change trend of ILSS values with the moisture absorption of pultruded GFRP composites,

Table 4 Short-beam-shear test characteristics

Time period (days)	Deionized water						Saltwater					
	30 ± 1 °C			60 ± 1 °C			30 ± 1 °C			60 ± 1 °C		
	Strength (MPa)	S (MPa)	Retention (%)	Strength (MPa)	S (MPa)	Retention (%)	Strength (MPa)	S (MPa)	Retention (%)	Strength (MPa)	S (MPa)	Retention (%)
Unexposed SBS strength = 39.11 (MPa)												
15	40.76	0.70	104.21	36.48	0.59	93.26	38.99	0.43	99.68	39.25	0.59	100.35
30	40.12	0.78	102.58	36.11	0.47	92.31	40.51	0.74	103.58	38.35	0.47	98.01
60	39.47	0.43	100.90	31.37	0.47	80.20	40.94	0.70	104.68	35.21	0.59	90.01
90	39.60	0.43	101.24	30.88	0.47	78.95	39.88	0.59	102.39	34.05	0.74	87.05
120	37.38	0.63	95.56	29.56	0.70	75.58	40.05	0.74	101.97	32.07	0.55	86.81
150	35.90	0.63	91.78	31.06	0.66	79.41	39.07	0.78	99.89	33.95	0.74	81.99
180	31.78	0.51	81.25	27.85	0.47	71.21	35.97	0.63	91.97	31.86	0.55	81.47

an approximate linear relationship could be found, which is described in form as

$$\frac{M_t}{M_\infty} = m\left(1 - \frac{(\tau_m)_t}{(\tau_m)_0}\right) \tag{13}$$

where M_t and M_∞ are the percentage moisture absorption levels at time t and saturation, respectively, $(\tau_m)_t$ and $(\tau_m)_0$ are the ILSS values at time t and 0 (unexposed condition), respectively, and m is a constant relating moisture content to deterioration. The saturation was not achieved in some tests, in case of immersed in deionized water at 30 ± 1 °C and 60 ± 1 °C. The M_∞ is defined as the maximum amount of absorption in those case. The term (M_t/M_∞) represents the degree of saturation, whereas the term $1 - (\tau_m)_t/(\tau_m)_0$ represents the fractional loss in strength at time t. The relationships between M_t/M_∞ and $1 - (\tau_m)_t/(\tau_m)_0$ of pultruded GFRP composites immersed in deionized and saltwater are shown in Figs. 14 and 15. The pultruded GFRP composites had a value of m of 0.022 and 0.027 immersed in 30 ± 1 °C and 60 ± 1 °C deionized water, respectively, whereas those had a value of m of 0.0138 and 0.0263 immersed in 30 ± 1 °C and 60 ± 1 °C saltwater, respectively, with corresponding correlation coefficients, R^2, of 0.53, 0.90, 0.44, and 0.95, respectively. It was noted that, as the increasing of temperature of solutions, the values of m were increased, which meant the higher speed of degradation. In addition, the values of R-square were also increased, expressed a better agreement with the test data.

Figures 16 and 17 show the effect of moisture absorption on the relative inter-laminar shear strength (τ_m/τ_{m0}, where τ_m and τ_{m0} are the inter-laminar shear strengths of the aged and un-aged specimens, respectively) and the relative interfacial shear strength (τ_i/τ_{i0}, where τ_i and τ_{i0} are the respective interfacial and shear strengths of the aged and un-aged specimens) of pultruded GFRP composites in water immersion condition. As shown in Fig. 16a, in addition to the rising stage of relative shear strength, the ratio τ_m/τ_{m0} of the specimen varied from 1.04 when $M_t = 1$ to 0.81 when $M_t = 1.31$. The change trend of τ_m/τ_{m0} was similar to that of τ_i/τ_{i0}. The value of τ_i/τ_{i0} for the specimen varied from 1.17 when $M_t = 0.87$, down to 0.79 when $M_t = 1.31$. As shown in Fig. 16b, the value of τ_m/τ_{m0} for the specimen varied from 1 at $M_t = 0$ to 0.71 at $M_t = 1.48$. The value τ_i/τ_{i0} for the specimen varies from 1 at $M_t = 0$ to 0.47 at

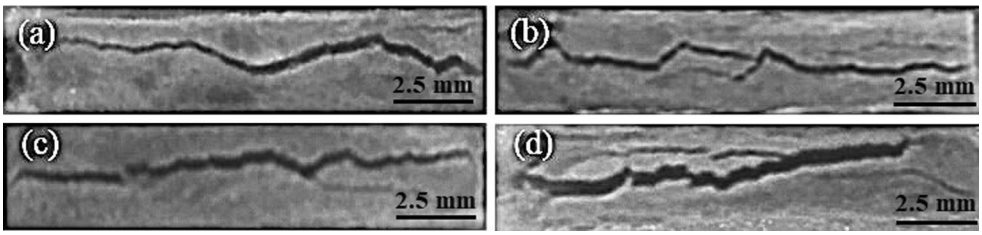

Figure 10 Typical failure images of pultruded GFRP composites in SBS test exposed in deionized water: **a** 30 ± 1 °C, 30 days, **b** 30 ± 1 °C, 180 days, **c** 60 ± 1 °C, 30 days, and **d** 60 ± 1 °C, 180 days.

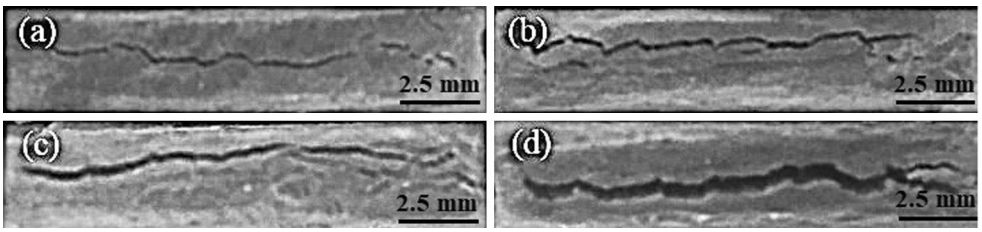

Figure 11 Typical failure images of pultruded GFRP composites in SBS test exposed in saltwater: **a** 30 ± 1 °C, 30 days, **b** 30 ± 1 °C, 180 days, **c** 60 ± 1 °C, 30 days, and **d** 60 ± 1 °C, 180 days.

Table 5 Characteristics of single-fiber-fragment test

Immersion conditions	Strain F (N)	S(N)	Number of fiber breaks	Max. length L_{max} (μm)	Min. length L_{min} (μm)	Average length L_{ave} (μm)	S (μm)
Unexposed	250.24	10.51	9	1134	854	976	199
30 ± 1 °C deionized water	209.82	8.18	5	1643	895	1235	376
60 ± 1 °C deionized water	183.95	11.88	3	2420	1628	2081	400
30 ± 1 °C saltwater	242.61	10.43	7	1235	597	980	326
60 ± 1 °C saltwater	218.64	7.65	6	2081	783	1273	571

Table 6 Interfacial shear strength (IFSS) characteristics

Time period (days)	30 ± 1 °C deionized water	S (MPa)	60 ± 1 °C deionized water	S (MPa)	30 ± 1 °C saltwater	S (MPa)	60 ± 1 °C saltwater	S (MPa)
Unexposed IFSS = 32.42 (MPa)								
15	31.15	0.81	27.44	1.78	32.11	1.75	27.81	1.95
30	32.23	2.83	27.35	1.69	34.89	2.01	27.87	1.64
60	29.98	0.81	22.81	1.69	29.51	2.04	25.45	2.14
90	26.39	1.88	18.49	1.75	29.21	1.95	24.88	1.65
120	25.02	1.59	16.83	1.72	27.99	2.24	22.71	2.01
150	23.59	1.98	13.83	1.75	28.05	1.95	21.67	1.78
180	21.80	1.23	12.94	2.30	27.48	2.04	21.15	1.65

M_t = 1.48. Figure 17 shows that M_t and τ_m/τ_{m0} have the same relationship as M_t and τ_i/τ_{i0}. The results indicated that moisture absorption can reflect the values of inter-laminar shear strength (ILSS) and interfacial shear strength (IFSS), and the decrease in the strength of the interface was directly caused by

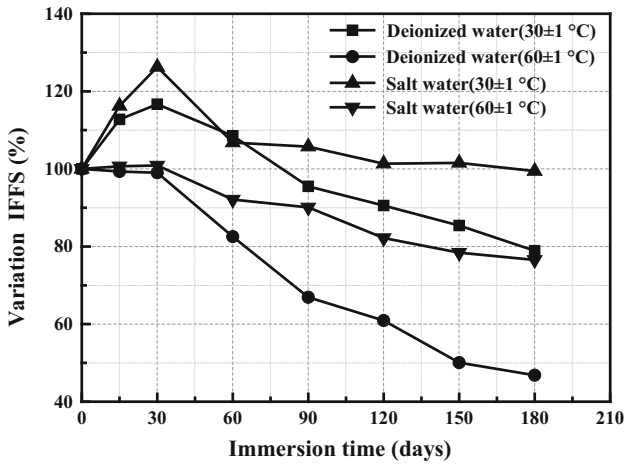

Figure 12 Interfacial shear strength (IFSS) of pultruded GFRP composites vs. immersion time for deionized water immersion and saltwater immersion.

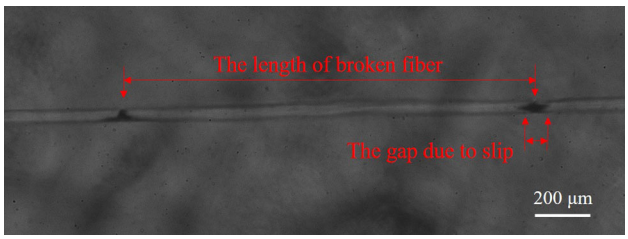

Figure 13 Images of specimen failure mode after single-fiber-fracture test.

moisture absorption. It was noted that IFSS was more sensitive to moisture absorption than ILSS. For the SFFT specimens, there was a higher diffusion rate in the fiber direction because the fiber ends were exposed directly to water, which allowed moisture wicking along the fiber/matrix interface, establishing intermolecular hydrogen bonding with fibers and reducing interfacial adhesion of the fiber/matrix [37]. It can be seen that the decrease of micro-interfacial bond strength was the direct reason for the change of mechanical properties. Furthermore, the decrease of macro-interfacial bond strength was the accumulation of the debonding of the micro-interface.

Morphology analysis

To determine whether water immersion caused any physical damage to pultruded GFRP composites, the specimen surface microstructure was examined by SEM for immersion durations of 0, 30, 90, and 180 days, respectively. Typical images of the control specimens are presented in Figs. 18a and 19a. No evidence of degradation was observed on the glass fiber and fiber/matrix interface when the face sheets immersed in deionized water and saltwater after 30 days, as shown in Figs. 18b and 19b. Additionally, the polymer started to deteriorate and more and more gaps observed between fiber and resin as the exposure time increased. It was possible to observe that debonding occurred between fiber and resin, and consequent fiber pullout when aging time increased, as shown in Figs. 18c, d, 19c, d. Compared to Figs. 18c, d, 19c, d, it could be obvious that the effect of deionized water on degradation was more than that of saltwater. The SEM results were consistent with the tensile and interface test results. In addition, Aldajah et al. [38] pointed out that the mechanical properties and the final failure of the composite system were significantly affected by the debonding between the fiber and matrix.

FTIR analysis

FTIR analysis was also used to better understand whether the degradation reaction could take place after hygrothermal aging. Figure 20 shows FTIR spectra of pultruded GFRP composite aged at different temperatures. It was noted that the resin did not degrade chemically during the immersion in deionized water after 180 days of aging at 30 ± 1 °C. However, the increases in the intensity of the peaks at 1700 cm^{-1} were observed for specimens aged with higher temperature. This can be related to the formation of carboxyl (–COOH), and the break of hydroxyl (–OH), which explains the occurrence of hydrolytic decomposition of resin matrix of composite under water immersion [39]. In addition, changes in the form of the peaks at 1250 cm^{-1} and 950 cm^{-1} were observed. These changes in the FTIR spectra can be attributed to a dehydration reaction following hydrolysis [40]. Similar behaviors are exhibited in FTIR spectra in saltwater conditions (Fig. 21). The findings suggested that the negative effect on resin in saltwater condition was mainly caused by water, and the salt did not react with the resin. At the same time, the increase of temperature would accelerate the degree of hydrolysis reaction. These observations from the FTIR analysis can explain the causes of the above-mentioned changes in the mechanical properties and microstructures of specimens.

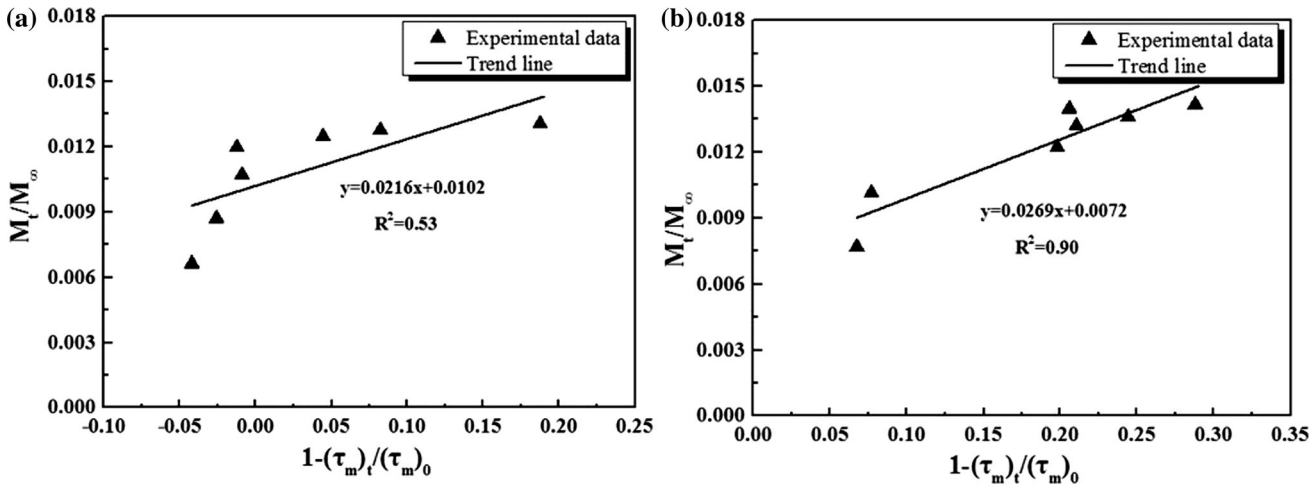

Figure 14 Regression of degree of saturation and relative inter-laminar shear strength of pultruded GFRP composites immersed in deionized water: **a** 30 ± 1 °C and **b** 60 ± 1 °C.

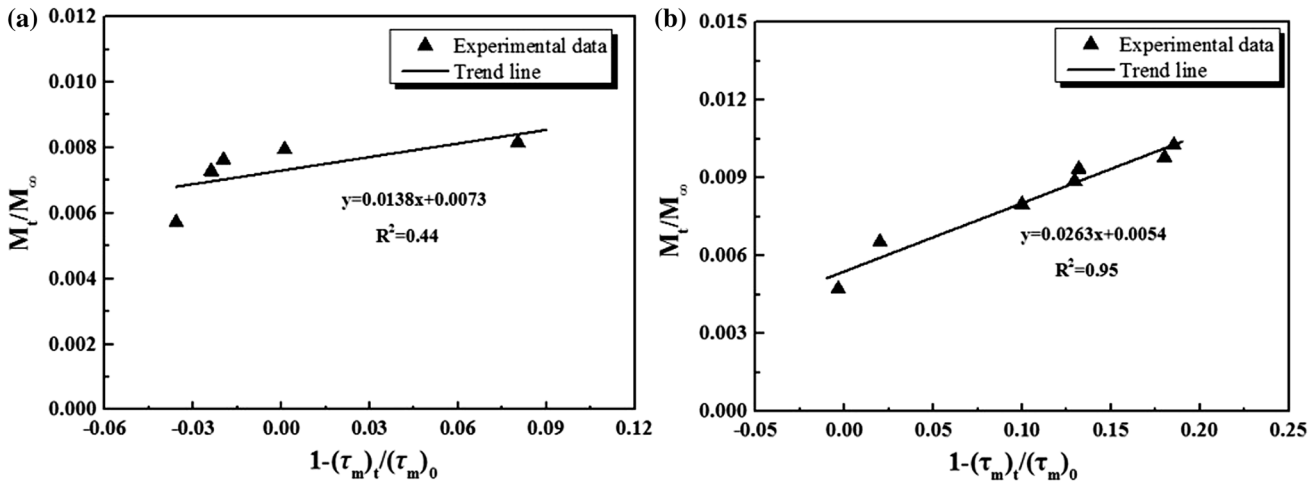

Figure 15 Regression of degree of saturation and relative inter-laminar shear strength of pultruded GFRP composites immersed in saltwater: **a** 30 ± 1 °C and **b** 60 ± 1 °C.

Prediction of *F*–ε of pultruded GFRP composites

The sharp and scale parameters of Weibull distribution can be estimated based on the single-fiber-fragment test. Then, according to Eq. (1), the probability density function is given as

$$p_f(\sigma_f) = L\sigma_0^{-\alpha}\alpha\sigma_f^{\alpha-1}\exp\left[-L\left(\frac{\sigma_f}{\sigma_0}\right)^{\alpha}\right] \tag{14}$$

And according to Eq. (14), the average strength of fiber ($\overline{\sigma_f}$) is given as

$$\overline{\sigma_f} = \int_0^{\infty}\sigma_f p_f(\sigma_f)d\sigma_f = \sigma_0 L^{-1/\alpha}\Gamma\left(1+\frac{1}{\alpha}\right) \tag{15}$$

By taking natural logarithms on both sides of Eq. (15), the ln $\overline{\sigma_f}$—ln L relationship is linearized with $-1/\alpha$ *as* the slope. Take the single-fiber-fragment test in 60 ± 1 °C deionized water condition after 0 day and 180 days to be an example, the sharp parameters are 3.008 and 4.152, respectively, as shown in Fig. 22.

It is assumed that the width and thickness of pultruded GFRP profiles are W and H, and the fibers were placed as a hexagonal array (Fig. 23). Then, the total number of fibers in pultruded GFRP composites can be expressed as

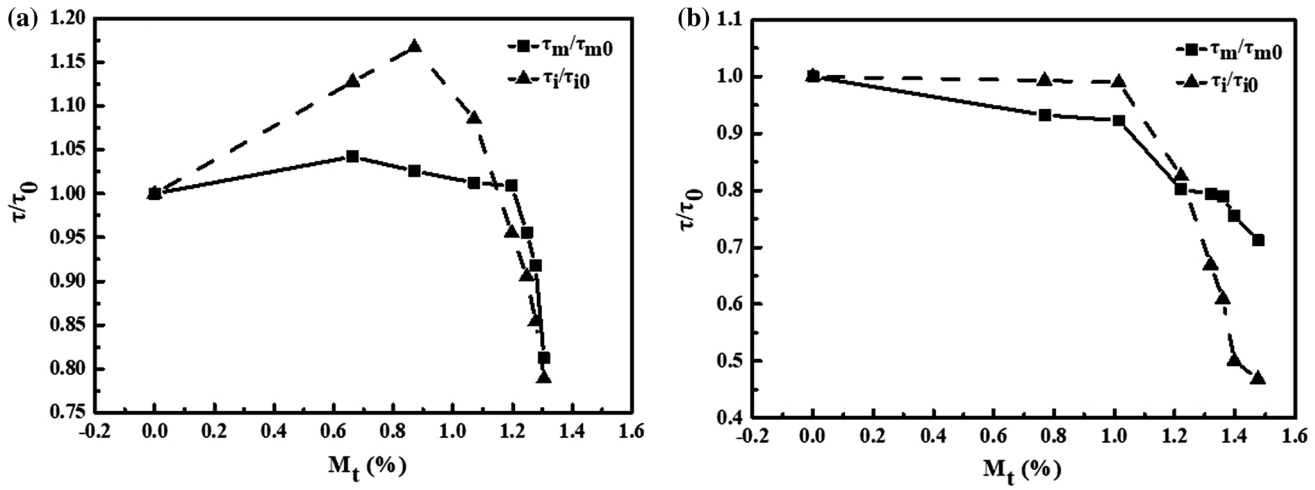

Figure 16 Effect of moisture absorption on the relative shear strength of pultruded GFRP composites immersed in deionized water: **a** 30 ± 1 °C and **b** 60 ± 1 °C.

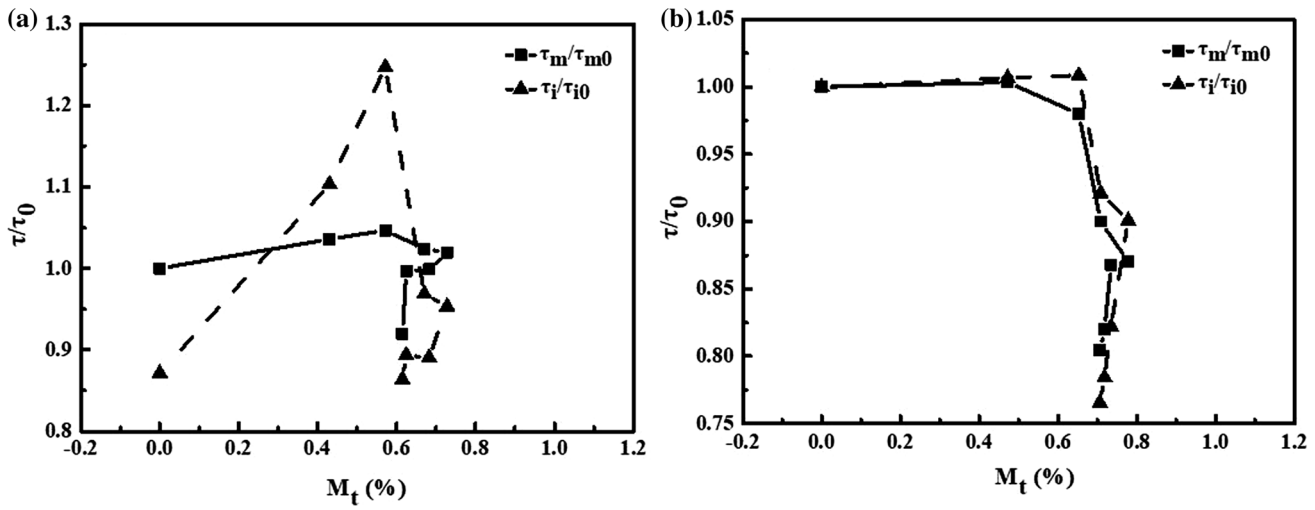

Figure 17 Effect of moisture absorption on the relative shear strength of pultruded GFRP composites immersed in saltwater: **a** 30 ± 1 °C and **b** 60 ± 1 °C.

$$N = N_1 \times N_2 = \frac{W}{d'} \times \frac{H}{d'} \tag{16}$$

$$d\prime = 2.1992 \sin(60) r_f / \sqrt{V_f} \tag{17}$$

where d' is the space between fibers, r_f is the radius of fiber, V_f is the volume ratio of the fibers. The radius and elastic modulus of fiber are 12 μm and 73 GPa, respectively. The shear modulus and elastic modulus of matrix are 10 MPa and 2.3 GPa. A series of parameters are derived from the above material property data: d' = 0.0177 mm, $N_1 \approx 1413$, $N_2 \approx 153$. Thus, the total number of fibers in a pultruded GFRP composite is given as 216189.

A relationship between the mean value (μ), the shape factor (α), and the scale factor (β) can be expressed as

$$\mu = \beta \Gamma\left(1 + \frac{1}{\alpha}\right) \tag{18}$$

The term determined by the gamma function in Eq. (18) is equal to 0.8931 for α = 3.008 and 0.9083 for α = 4.1528. Thus, the scale factor can be directly approximated by the expected value (β = 9.65, when α = 3.008; β = 9.23, when α = 4.1528).

Based on Eq. (6), the curves of F–ε_f are given. Figure 24 shows the changes in value of tensile force of pultruded GFRP composites immersed in 60 °C

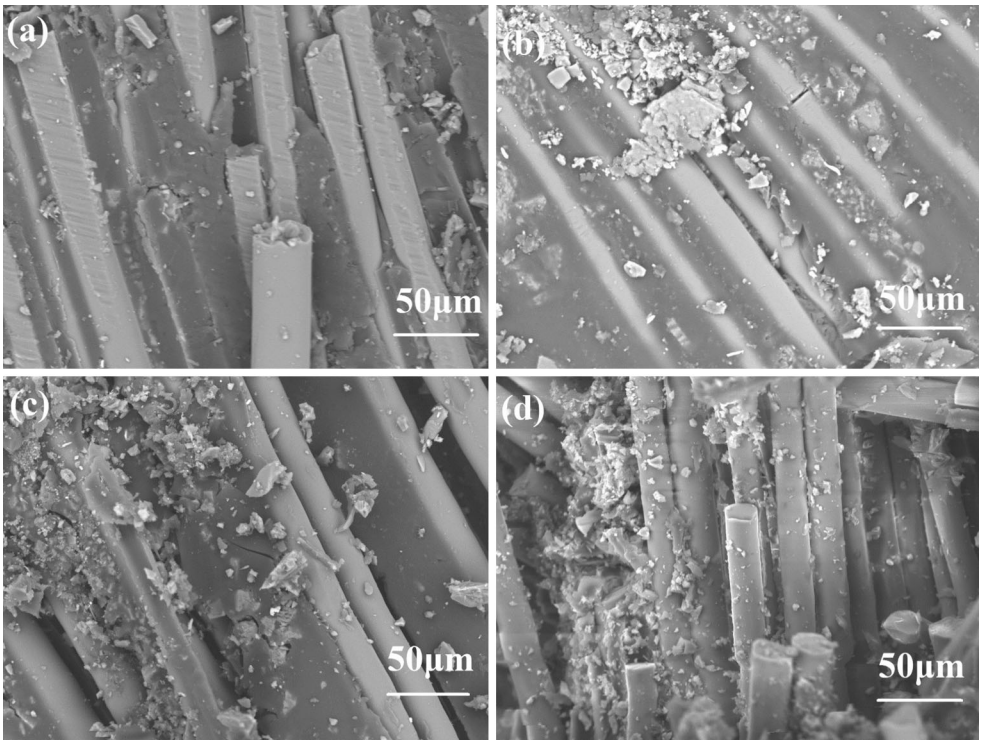

Figure 18 SEM micrographs of pultruded GFRP composite surfaces at different immersion time: **a** 0 day, **b** 30 days, **c** 90 days, and **d** 180 days for deionized water immersion at 20 ± 5 °C.

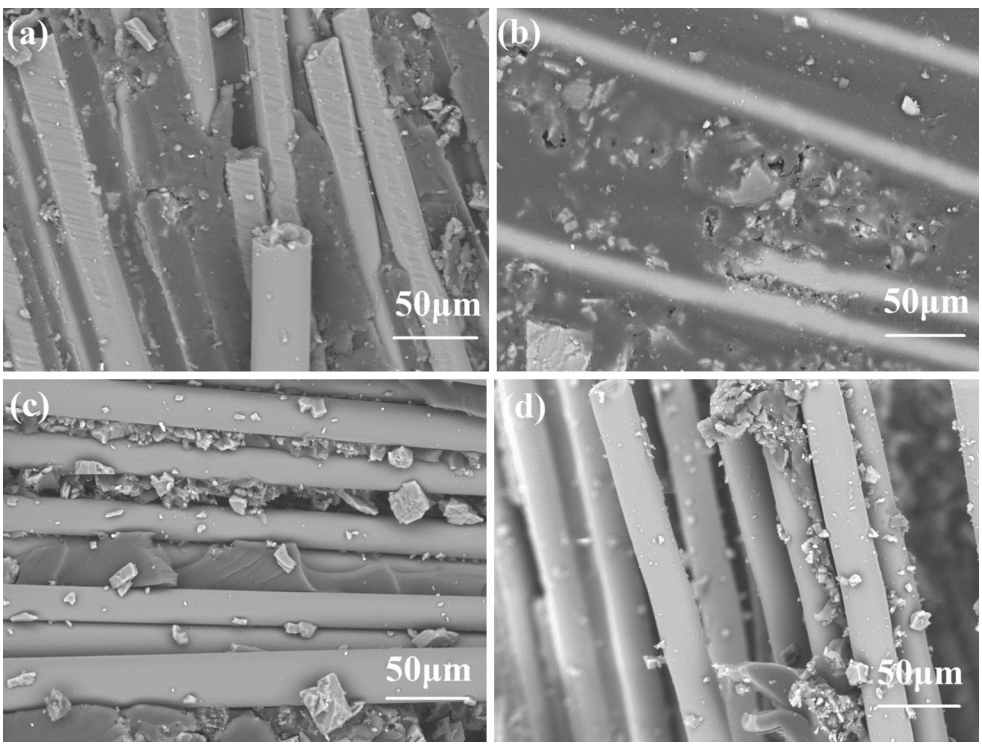

Figure 19 SEM micrographs of pultruded GFRP composite surfaces at different immersion time: **a** 0 day, **b** 30 days, **c** 90 days, and **d** 180 days for saltwater immersion at 20 ± 5 °C.

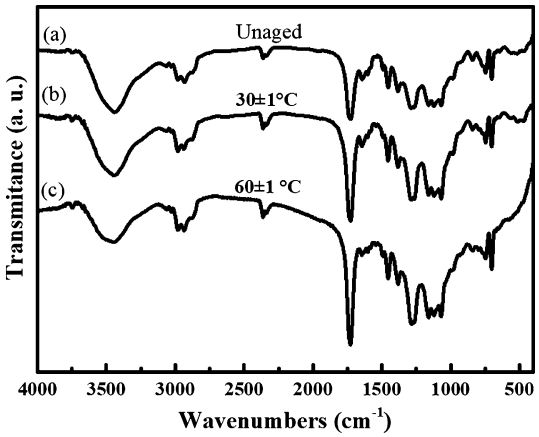

Figure 20 FTIR spectra of pultruded GFRP composites at different immersion temperatures before and after 180 days of aging in deionized water.

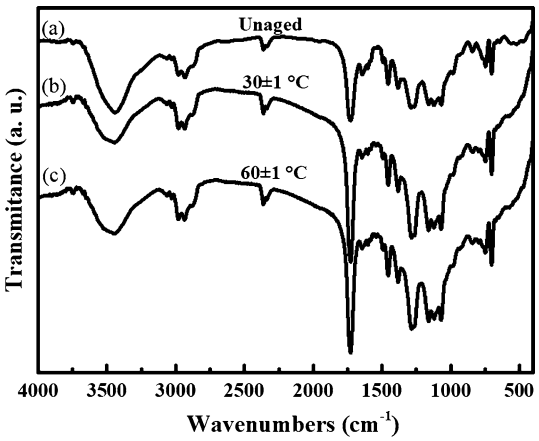

Figure 21 FTIR spectra of pultruded GFRP composites at different immersion temperatures after 180 days of aging for saltwater.

deionized water after 0 day and 180 days. It was noted that, at the initial stage, the maximum bearing capacity of pultruded GFRP composites was 49.05 kN, and the maximum strain was 0.077 μm. After 180-day immersion, the maximum bearing capacity of pultruded GFRP composites declined to 46.78 kN, which represented approximately 6% level of degradation. Also, the value of maximum strain presented a downward trend, and that was 0.073 μm. Comparing the analytical and experimental results indicates that the proposed tensile force of pultruded GFRP composites based on interfacial strength is able to match the experiment data well.

Conclusions

This paper presents the durability of pultruded GFRP composites immersed in saltwater and deionized water at different temperatures. The study focused on the moisture absorption kinetics of pultruded GFRP composites, and the effects of moisture absorption on mechanical properties such as tensile properties and the macro- and micro-interfacial strength. Based on the above study, the main findings of this study are summarized as follows:

1. The moisture absorption of pultruded GFRP composites increased nonlinearly as the temperature rose. Elevating the temperature increased the moisture absorption capacity and diffusion coefficient of the pultruded GFRP composites in both deionized water and saltwater conditions. The equilibrium moisture absorption of specimens in saltwater was slightly less than that of specimens immersed in water at the same temperature because of the high concentration of dissolved particles in saltwater that retard moisture diffusion by osmosis.
2. After 180 days of aging, the losses of tensile strength and modulus were, respectively, 25.7% and 26% for specimens immersed in deionized water at 20 ± 5 °C, whereas the equivalent respective losses were 2.1% and 18.2% for specimens immersed in saltwater at 20 ± 5 °C. The results indicated that higher moisture absorption caused more drastic degradation in tensile properties.
3. As the inter-laminar shear strength of specimens after 180-day immersion in deionized water and saltwater decreased 18.8% and 8.9%, respectively, at 30 ± 1 °C, and 28.8% and 18.5%, respectively, at 60 ± 1 °C. The values of interfacial shear strength decreased were 21.1, 0.6, 53.2, and 23.5%, respectively, at the same condition. It was noted that the hydrolysis of resin and E-glass fibers and debonding at the interface were the major reasons for the degradation of tensile properties of GFRP composites.
4. The diffusion rate of micro-interface was higher than that of macro-interface in the fiber direction because of moisture wicking along the fiber/matrix interface, establishing intermolecular hydrogen bonding with fibers and reducing interfacial adhesion of the fiber/matrix.

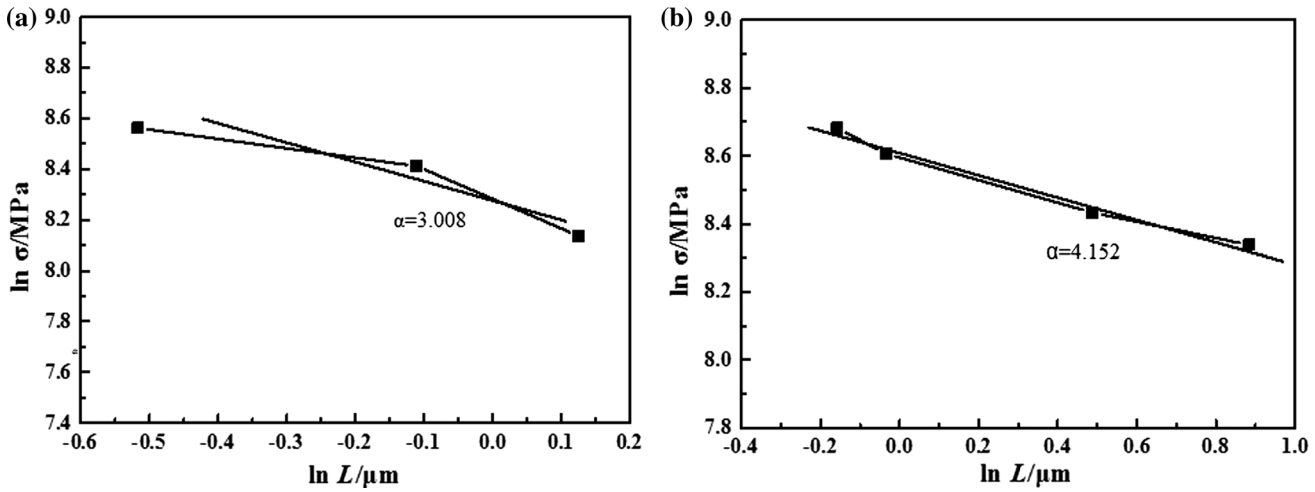

Figure 22 Relationship between average fracture strength and length of E-glass fiber exposed in 60 ± 1 °C deionized water at different immersion time: **a** 0 day and **b** 180 days.

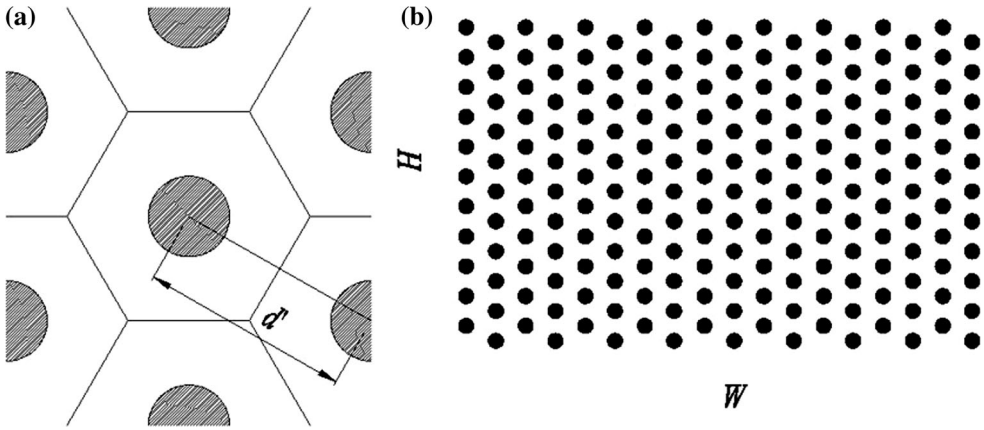

Figure 23 Calculation models for the geometry parameter of microstructure of pultruded GFRP composites: **a** calculation model for fiber spacing and **b** calculation model for total number of fibers in a pultruded GFRP composite.

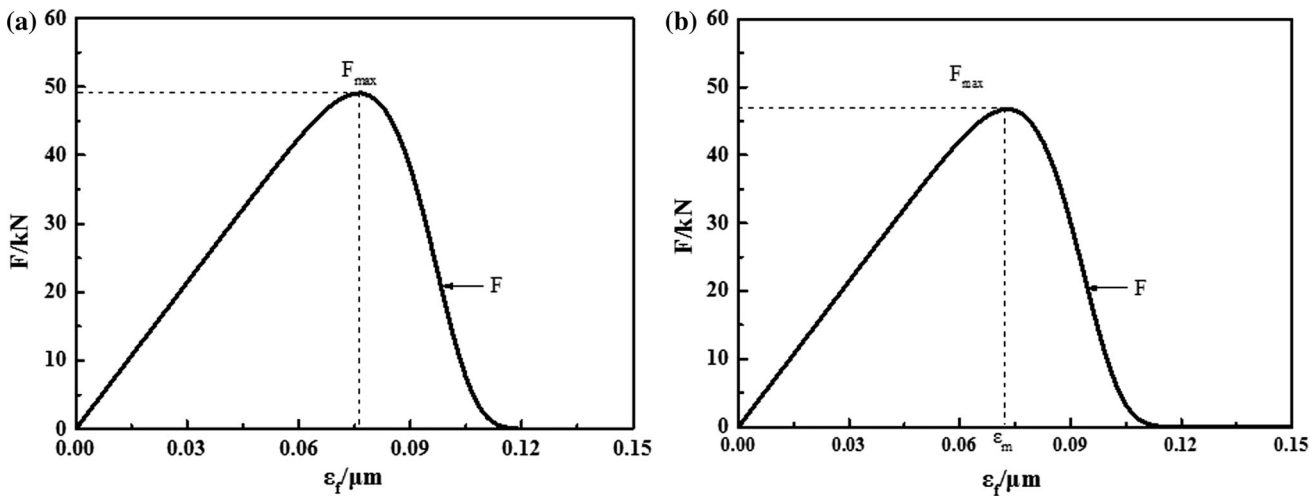

Figure 24 Cures of F–ε_f of pultruded GFRP profiles exposed in deionized water after **a** 0 day and **b** 180 days.

5. A numerical method, based on the change of interfacial strength and Weibull distribution, was proposed to describe the temperature effects on pultruded GFRP composites. Moreover, the degradation trends of ultimate bearing capacity of pultruded GFRP composites in hygrothermal environments were noted.

Acknowledgements

The authors gratefully acknowledge the financial support received from the National Natural Science Foundation of China (Grant Nos. 51608264 and 51778285) and Jiangsu Government Scholarship for Overseas Studies (Grant No. JS-2016-083).

References

[1] Fang Y, Chen P, Huo R, Liang Y, Wang L, Liu W (2018) Hygrothermal ageing of polymeric sandwich structures used in structural engineering. Constr Build Mater 165:818–824

[2] Feng J, Guo Z (2016) Effect of temperature and frequency on dynamic mechanical properties of glass/epoxy composites. J Mater Sci 51:2747–2758. https://doi.org/10.1007/s10853-015-9589-5

[3] Sousa J-M, Correia J-R, Cabral-Fonseca S (2016) Durability of glass fibre reinforced polymer pultruded profiles: comparison between QUV accelerated exposure and natural weathering in a mediterranean climate. Exp Tech 40:207–219

[4] Grammatikos S-A, Evernden M, Mitchels J, Zafari B, Mottram J-T (2016) On the response to hygrothermal aging of pultruded FRPs used in the civil engineering sector. Mateer Des 96:283–295

[5] Sousa J-M, Correia J-R, Cabral-Fonseca S, Diogo A-C (2014) Effects of thermal cycles on the mechanical response of pultruded GFRP profiles used in civil engineering applications. Compos Struct 116(1):720–731

[6] Wang J, Zhou W, Luo F, Zhu D, Qing Y (2017) Mechanical performance of nanosilica filled quartz fiber/polyimide composites at room and elevated temperatures. J Mater Sci 52(20):12207–12220. https://doi.org/10.1007/s10853-017-1341-x

[7] Feng P, Wang J, Wang Y, Loughery D, Niu D (2014) Effects of corrosive environments on properties of pultruded GFRP plates. Compos Part B 67:427–433

[8] Repon M-R-U, Motaleb K-Z-M-A, Islam M-T, Mamun R-A, Mithu M-M-R (2017) Tensile and water absorption properties of jute and pineapple fabric reinforced polyester composite. Int J Compos Mater 7(2):72–76

[9] Silva M-A-G, Fonseca B-S-D, Biscaia H (2014) On estimates of durability of FRP based on accelerated tests. Compos Struct 116(9):377–387

[10] Guermazi N, Tarjem A-B, Ksouri I, Ayedi H-F (2016) On the durability of FRP composites for aircraft structures in hygrothermal conditioning. Compos Part B 85:294–304

[11] Gu Y, Liu H, Li M, Li Y, Zhang Z (2014) Macro- and micro-interfacial properties of carbon fiber reinforced epoxy resin composites under hygrothermal treatments. J Reinf Plast Compos 33(4):369–379

[12] Ramirez F-A, Carlsson L-A, Acha B-A (2008) Evaluation of water degradation of vinylester and epoxy matrix composites by single fiber and composite tests. J Mater Sci 43(15):5230–5242. https://doi.org/10.1007/s10853-008-2766-z

[13] Chin J-W, Nguyen T, Aouadi K (2015) Sorption and diffusion of water, salt water, and concrete pore solution in composite matrices. J Appl Polym Sci 71(3):483–492

[14] ASTM International (2014) Standard test method for moisture absorption properties and equilibrium conditioning of polymer matrix composite materials. ASTM D5229/D5229M, ASTM International, West Conshohocken, PA

[15] ASTM International (2014) Standard test method for tensile properties of polymer matrix composite materials. ASTM D3039/D3039M-14, ASTM International, West Conshohocken, PA

[16] Whitney J-M, Browning C-E (1985) On short-beam shear tests for composite materials. Exp Mech 25(3):294–300

[17] ASTM International (2015) Standard test method for short-beam strength of polymer matrix composite materials and their laminates. ASTM D2344/D2344M, ASTM International, West Conshohocken, PA

[18] Kelly A, Tyson W-R (1965) Tensile properties of fiber-reinforced metals: copper/tungsten and copper/molybdenum. J Mech Phys Solids 13:329–350

[19] Karbhari V-M, Abanilla M-A (2007) Design factors, reliability, and durability prediction of wet layup carbon/epoxy used in external strengthening. Compos Part B 38(1):10–23

[20] Sethi S, Ray B-C (2015) Environmental effects on fibre reinforced polymeric composites: evolving reasons and remarks on interfacial strength and stability. Adv Colloid Interface Sci 217:43–67

[21] Fang Y, Wang K, Hui D, Xu F, Liu W, Yang S, Wang L (2017) Monitoring of seawater immersion degradation in glass fibre reinforced polymer composites using quantum dots. Compos Part B 112:93–102

[22] Meng M, Le H, Grove S, Rizvi M-J (2016) Moisture effects on the bending fatigue of laminated composites. Compos Struct 154:49–60

[23] Xian G, Li H, Su X (2012) Water absorption and hygrothermal aging of ultraviolet cured glass-fiber reinforced acrylate composites. Polym Compos 33(7):1120–1128

[24] Firdosh S, Murthy H-N-N, Pal R, Angadi G, Raghavendra N (2015) Durability of GFRP nano-composites subjected to hygrothermal aging. Compos Part B 69(69):443–451

[25] Xin H, Liu Y, Mosallam A, Zhang Y (2016) Moisture diffusion and hygrothermal aging of pultruded glass fiber reinforced polymer laminates in bridge application. Compos Part B 100:197–207

[26] Shen C-H, Springer G-S (1976) Moisture absorption and desorption of composite materials. J Compos Mater 10(1):2–20

[27] Yang Q, Xian G, Karbhari V-M (2008) Hygrothermal aging of an epoxy adhesive used in FRP strengthening of concrete. J Appl Polym Sci 107(4):2607–2617

[28] Karbhari V-M (2004) E-glass/vinylester composites in aqueous environments: effects on short-beam shear strength. J Compos Constr 8(2):148–156

[29] Valadez-Gonzalez A, Cervantes-Uc J-M, Olayo R, Herrera-Franco P-J (1999) Effect of fiber surface treatment on the fiber-matrix bond strength of natural fiber reinforced composites. Compos Part B 30(30):309–320

[30] Chu W, Wu L, Karbhari V-M (2004) Durability evaluation of moderate temperature cured E-glass/vinylester systems. Compos Struct 66(1):367–376

[31] Abanilla M-A, Li Y, Karbhari V-M (2006) Durability characterization of wet layup graphite/epoxy composites used in external strengthening. Compos Part B 37(2–3):200–212

[32] Duigou A-L, Davies P, Baley C (2013) Exploring durability of interfaces in flax fibre/epoxy micro-composites. Compos A Appl Sci Manuf 48(1):121–128

[33] Kafodya I, Xian G, Li H (2014) Durability study of pultruded CFRP plates immersed in water and seawater under sustained bending: water uptake and effects on the mechanical properties. Compos Part B 70:138–148

[34] Marouani S, Curtil L, Hamelin P (2012) Aging of carbon/epoxy and carbon/vinylester composites used in the reinforcement and/or the repair of civil engineering structures. Compos Part B 43(4):2020–2030

[35] Zheng X-H, Huang P-Y, Guo X-Y, Huang J-L (2016) Experimental study on bond behavior of FRP-concrete interface in hygrothermal environment. Int J Polym Sci 2016(5):1–12

[36] Sawpan M-A, Mamun A-A, Holdsworth P-G (2014) Long term durability of pultruded polymer composite rebar in concrete environment. Mater Des 57(5):616–624

[37] Han K-L, Kim D-S, Won J-S, Da Y-J, Lee HJ (2016) Effects of thermal and humidity aging on the interfacial adhesion of polyketone fiber reinforced natural rubber. Compos Adv Mater Sci Eng 2016:1–8

[38] Aldajah S, Alawsi G, Rahmaan S-A (2009) Impact of sea and tap water exposure on the durability of GFRP laminates. Mater Des 30(5):1835–1840

[39] Mourad A-H-I, Abdel-Magid B-M, EI-Maaddawy T, Grami ME (2010) Effect of seawater and warm environment on glass/epoxy and glass polyurethane composites. Appl Compos Mater 17(5):557–573

[40] Ghorbel I, Valentin D (1993) Hydrothermal effects on the physic-chemical properties of pure and glass fiber reinforced polyester and vinylester resins. Polym Compos 14(4):324–334

Terms and Conditions

Springer Nature journal content, brought to you courtesy of Springer Nature Customer Service Center GmbH (“Springer Nature”).
Springer Nature supports a reasonable amount of sharing of research papers by authors, subscribers and authorised users (“Users”), for small-scale personal, non-commercial use provided that all copyright, trade and service marks and other proprietary notices are maintained. By accessing, sharing, receiving or otherwise using the Springer Nature journal content you agree to these terms of use (“Terms”). For these purposes, Springer Nature considers academic use (by researchers and students) to be non-commercial.
These Terms are supplementary and will apply in addition to any applicable website terms and conditions, a relevant site licence or a personal subscription. These Terms will prevail over any conflict or ambiguity with regards to the relevant terms, a site licence or a personal subscription (to the extent of the conflict or ambiguity only). For Creative Commons-licensed articles, the terms of the Creative Commons license used will apply.
We collect and use personal data to provide access to the Springer Nature journal content. We may also use these personal data internally within ResearchGate and Springer Nature and as agreed share it, in an anonymised way, for purposes of tracking, analysis and reporting. We will not otherwise disclose your personal data outside the ResearchGate or the Springer Nature group of companies unless we have your permission as detailed in the Privacy Policy.
While Users may use the Springer Nature journal content for small scale, personal non-commercial use, it is important to note that Users may not:

1. use such content for the purpose of providing other users with access on a regular or large scale basis or as a means to circumvent access control;
2. use such content where to do so would be considered a criminal or statutory offence in any jurisdiction, or gives rise to civil liability, or is otherwise unlawful;
3. falsely or misleadingly imply or suggest endorsement, approval , sponsorship, or association unless explicitly agreed to by Springer Nature in writing;
4. use bots or other automated methods to access the content or redirect messages
5. override any security feature or exclusionary protocol; or
6. share the content in order to create substitute for Springer Nature products or services or a systematic database of Springer Nature journal content.

In line with the restriction against commercial use, Springer Nature does not permit the creation of a product or service that creates revenue, royalties, rent or income from our content or its inclusion as part of a paid for service or for other commercial gain. Springer Nature journal content cannot be used for inter-library loans and librarians may not upload Springer Nature journal content on a large scale into their, or any other, institutional repository.
These terms of use are reviewed regularly and may be amended at any time. Springer Nature is not obligated to publish any information or content on this website and may remove it or features or functionality at our sole discretion, at any time with or without notice. Springer Nature may revoke this licence to you at any time and remove access to any copies of the Springer Nature journal content which have been saved.
To the fullest extent permitted by law, Springer Nature makes no warranties, representations or guarantees to Users, either express or implied with respect to the Springer nature journal content and all parties disclaim and waive any implied warranties or warranties imposed by law, including merchantability or fitness for any particular purpose.
Please note that these rights do not automatically extend to content, data or other material published by Springer Nature that may be licensed from third parties.
If you would like to use or distribute our Springer Nature journal content to a wider audience or on a regular basis or in any other manner not expressly permitted by these Terms, please contact Springer Nature at

onlineservice@springernature.com